nature medicine

Clonal analyses and gene profiling identify genetic biomarkers of the thermogenic potential of human brown and white preadipocytes

Ruidan Xue[1,2], Matthew D Lynes[1], Jonathan M Dreyfuss[3,4], Farnaz Shamsi[1], Tim J Schulz[1], Hongbin Zhang[1], Tian Lian Huang[1], Kristy L Townsend[1], Yiming Li[2], Hirokazu Takahashi[1], Lauren S Weiner[1], Andrew P White[5], Maureen S Lynes[6,7], Lee L Rubin[6,7], Laurie J Goodyear[1], Aaron M Cypess[1,8] & Yu-Hua Tseng[1,7]

Targeting brown adipose tissue (BAT) content or activity has therapeutic potential for treating obesity and the metabolic syndrome by increasing energy expenditure. However, both inter- and intra-individual differences contribute to heterogeneity in human BAT and potentially to differential thermogenic capacity in human populations. Here we generated clones of brown and white preadipocytes from human neck fat and characterized their adipogenic and thermogenic differentiation. We combined an uncoupling protein 1 (UCP1) reporter system and expression profiling to define novel sets of gene signatures in human preadipocytes that could predict the thermogenic potential of the cells once they were maturated. Knocking out the positive UCP1 regulators, *PREX1* and *EDNRB*, in brown preadipocytes using CRISPR-Cas9 markedly abolished the high level of UCP1 in brown adipocytes differentiated from the preadipocytes. Finally, we were able to prospectively isolate adipose progenitors with great thermogenic potential using the cell surface marker CD29. These data provide new insights into the cellular heterogeneity in human fat and offer potential biomarkers for identifying thermogenically competent preadipocytes.

Obesity, mainly characterized by increased adiposity, has reached pandemic proportions and is a major contributor to metabolic disorders. In mammals, there are two functionally distinct types of fat: white adipose tissue (WAT), which is specialized for energy storage, and BAT, which dissipates energy for thermogenesis[1,2] via the activity of UCP1. In addition to the classical brown adipocytes, UCP1-positive 'beige' or 'brite' adipocytes can be recruited within WAT upon chronic cold or β3-adrenergic stimulation[3–6].

Because of the immense capacity of BAT to combust fuels for heat production[7,8] and owing to its presence in adult humans[9–14], increasing the amount or activity of brown or beige fat has been considered an appealing approach for the treatment or prevention of obesity and related metabolic disorders. Indeed, in rodents the activation of brown or beige fat can increase energy expenditure and is protective against diet-induced obesity[5,6,15]. In humans, BAT mass or activity is inversely correlated to body mass index and percentage of body fat[10–12], and cold exposure can elevate BAT volume and activity and increase energy expenditure, thus pointing toward the therapeutic potential of BAT in humans for the treatment of obesity and metabolic disease[16–18].

Recent data indicate that the neck, supraclavicular and spinal cord regions of adult humans contain substantial deposits of UCP1-positive adipocytes[19–22]. The presence of brown, beige, and white adipocytes, and possibly other unidentified adipose cell types, highlights the heterogeneity of adipose tissue depots, which is potentially related to their diverse functions in energy metabolism. Both inter-subject differences and various cellular compositions within a given fat tissue contribute to the heterogeneity of human BAT and affect thermogenic potential. In rodents, lineage tracing and cell sorting analyses have demonstrated that the various types of fat cells arise from discrete pools of progenitors, which express distinct molecular markers[19,23–26]. However, whether the markers identified in mouse cells can unambiguously define different types of human adipose progenitors is currently unknown.

A key impediment for these studies is the lack of human-derived brown and white fat progenitor cell models. To investigate the heterogeneous nature of the progenitor cell population in human BAT and WAT, we generated clonal cell lines from human neck fat and characterized their adipogenic differentiation and metabolic function *in vitro* and *in vivo* after transplantation into immune-deficient nude mice. Using clonal analysis and gene-expression profiling, we defined unique sets of gene signatures in human preadipocytes that could predict the thermogenic potential of these cells once they have

[1]Section on Integrative Physiology and Metabolism, Research Division, Joslin Diabetes Center, Harvard Medical School, Boston, Massachusetts, USA. [2]Division of Endocrinology and Metabolism, Huashan Hospital, Shanghai Medical College, Fudan University, Shanghai, China. [3]Bioinformatics Core, Joslin Diabetes Center, Harvard Medical School, Boston, Massachusetts, USA. [4]Department of Biomedical Engineering, Boston University, Boston, Massachusetts, USA. [5]Department of Orthopedic Surgery, Beth Israel Deaconess Medical Center, Harvard Medical School, Boston, Massachusetts, USA. [6]Department of Stem Cell and Regenerative Biology, Harvard University, Cambridge, Massachusetts, USA. [7]Harvard Stem Cell Institute, Harvard University, Cambridge, Massachusetts, USA. [8]Diabetes, Endocrinology, and Obesity Branch, National Institute of Diabetes and Digestive and Kidney Diseases, National Institutes of Health, Bethesda, Maryland, USA. Correspondence should be addressed to Y.-H.T. (yu-hua.tseng@joslin.harvard.edu).

Received 13 December 2014; accepted 19 May 2015; published online 15 June 2015; doi:10.1038/nm.3881

matured in culture into adipocytes. These data highlight the cellular heterogeneity in human BAT and WAT and provide novel gene markers that may be targeted or selected to prime preadipocytes for strong thermogenic differentiation.

RESULTS

Generation and characterization of human fat progenitors

We previously reported that adult human BAT and WAT are present in defined neck locations[20], and we found that deeper human neck fat is predominantly brown, as these depots express substantially higher levels of the brown fat–specific marker UCP1 compared to the depots of superficial neck fat. To define molecular and functional characteristics of specific adipose progenitors, we generated human preadipocyte cell populations derived from a total of four human subjects by isolating cells from the stromal vascular fraction (SVF) of human neck fat and immortalizing them via stable expression of human telomere reverse transcriptase (hTERT)[27] (**Supplementary Fig. 1a**). Pairs of immortalized progenitors for human BAT (hBAT-SVF cells, isolated from deep neck fat) and human WAT (hWAT-SVF cells, isolated from superficial neck fat) of the same individuals were established from each of the four individuals for proper comparisons (**Supplementary Table 1a**). The immortalized cells were passaged in culture for more than 90 d and were followed for up to 20 population doublings (**Supplementary Fig. 1b**).

After immortalization, the cells from both WAT and BAT depots of the four human subjects maintained a fibroblast-like morphology, and after induction with a standard adipogenic differentiation protocol most of the precursors became lipid-laden cells that highly expressed the mature adipocyte marker fatty acid synthase (*FASN*) (**Fig. 1a** and **Supplementary Fig. 1c**). Notably, in differentiated hBAT-SVF cells (referred to as human brown adipocytes, hBAs), expression of the brown fat marker *UCP1* was up to 200-fold higher than in differentiated hWAT-SVF cells (human white adipocytes, hWAs) (**Fig. 1b**), and was accompanied by robust induction of UCP1 protein (**Fig. 1c** and **Supplementary Fig. 1d**). A comparable pattern of expression was observed for other brown fat markers, such as

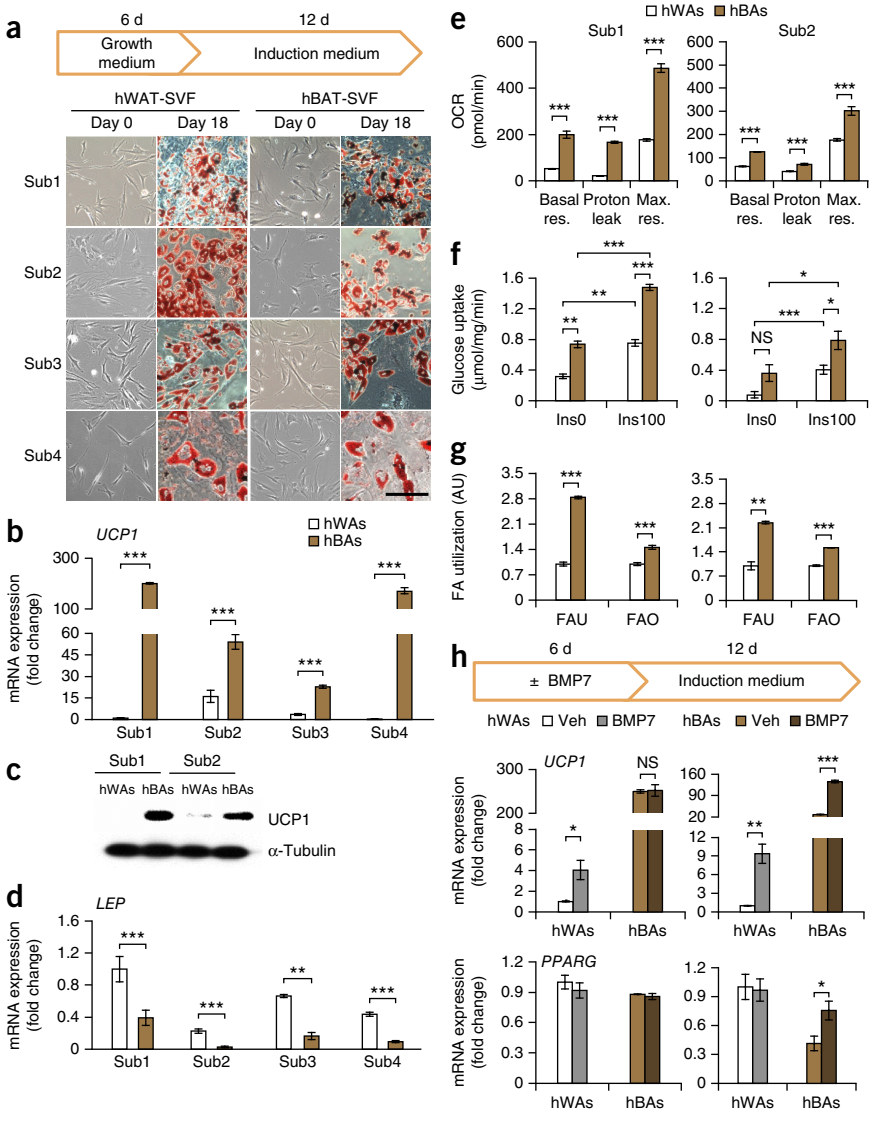

Figure 1 Generation and characterization of immortalized human brown and white fat progenitors. (**a**) Light microscopic images of immortalized human WAT progenitors (hWAT-SVF cells) and human BAT progenitors (hBAT-SVF cells) at day 0 and 18 (stained with Oil Red O) from four subjects (Sub1–4). Scale bar, 100 μm. (**b**) qRT-PCR analysis for *UCP1* mRNA expression in differentiated adipocytes from hWAT-SVF cells and hBAT-SVF cells from four subjects (Sub1–4). Data are presented as fold changes relative to subject1–derived hWAs ($n = 3$ per group, biological replicates). (**c**) Western blot analysis of UCP1 protein level in hWAs and hBAs differentiated from progenitors of Sub1 and Sub2. α-Tubulin serves as a loading control. (**d**) qRT-PCR analysis for *LEP* mRNA expression as in **b**. Data are presented as fold changes relative to subject1–derived hWAs ($n = 3$ per group, biological replicates). (**e**) Oxygen consumption rate (OCR) was measured in the absence (basal respiration, Basal res.) or presence of oligomycin (Proton leak) or FCCP (maximal respiration, Max. res.) in hWAs and hBAs from Sub1 (left) and Sub2 (right). Data are presented as mean ± s.e.m. ($n = 10$ per group, biological replicates; hWAs versus hBAs). (**f**) Glucose uptake was measured using [^{3}H]2-deoxy-glucose in hWAs and hBAs stimulated with (Ins100) or without (Ins0) 100 nM insulin from Sub1 (left) and Sub2 (right) ($n = 3$ per group, biological replicates). (**g**) Fatty acid uptake (FAU) and fatty acid oxidation (FAO) were measured using [^{14}C]palmitic acid in hWAs and hBAs from Sub1 (left) and Sub2 (right). Data are presented as fold change compared to FAU or FAO from hWAs ($n = 3$ per group, biological replicates). AU, arbitrary unit. (**h**) qRT-PCR analysis for *UCP1* and *PPARG* mRNA expression in hWAs and hBAs from Sub1 (left) and Sub2 (right). Data are presented as fold changes compared to mRNA expression in vehicle-treated (veh) hWAs for each subject ($n = 3$ per group, biological replicates; NS, not significant; Veh versus BMP7). Throughout, error bars represent mean ± s.e.m.; $^*P < 0.05$, $^{**}P < 0.01$, $^{***}P < 0.001$ by two-tailed Student's *t*-test. A representative experiment from a total of three independent studies is shown.

deiodinase 2 (*DIO2*) and peroxisome proliferator–activated receptor gamma coactivator 1 alpha (*PPARGC1A*) (**Supplementary Fig. 1c**). *LEP* (which encodes for leptin), a marker of WAT, was selectively expressed in hWAs compared to hBAs in all subjects (**Fig. 1d**). Importantly, the immortalized cells retained differentiation characteristics of primary cells (**Supplementary Fig. 2**).

To determine whether the differentiated cells possessed metabolic capacity, we evaluated cellular respiration and fuel utilization in hBAs and hWAs from two subjects (referred to herein as subjects 1 and 2). Consistent with differences in gene expression, the levels of basal and maximal respiration, as well as proton leak, in hBAs were higher compared to those in hWAs (**Fig. 1e**). Glucose uptake in both the basal and insulin-stimulated states was also notably higher in hBAs than in hWAs, as were both fatty acid uptake and oxidation rate (**Fig. 1f,g**). Differentiated brown, but not white, adipocytes were able to respond to forskolin, a chemical mimic of β-adrenergic stimulation, by increasing the oxygen consumption rate (**Supplementary Fig. 3a**). In addition, hBAs from subject 2 could respond to stimulations by norepinephrine and other browning agents by increasing the levels of *UCP1* and *DIO2* (**Supplementary Figs. 3b** and **4**), suggesting that the mature human brown adipocytes are responsive to both physiological and pharmacological adrenergic stimuli.

Recent studies using mouse systems have demonstrated that adipose progenitors can respond to inductive signals and increase their thermogenic capacity in mature adipocytes[4,23,28]. To determine whether human-derived progenitors can respond to browning agents, we pretreated the aforementioned precursors from subjects 1 and 2 with bone morphogenetic protein 7 (BMP7)[23,29] for 6 d, followed by adipogenic induction. Pre-exposure to BMP7 of hWAT-SVF cells from both subjects and hBAT-SVF cells from subject 2 led to increased *UCP1* expression, mitochondrial activity and fuel utilization in mature adipocytes (**Fig. 1h** and **Supplementary Fig. 5a–f**), suggesting that a fraction of these progenitors are inducible. Pretreatment with BMP7 also augmented peroxisome proliferator–activated receptor gamma (*PPARG*) expression in brown adipocytes from subject 2 only. BMP8, another browning agent[28], exerted similar effects (**Supplementary Fig. 5a**).

The fact that hBAT-SVF cells and hBAs derived from subject 2, but not subject 1, consistently responded to browning agents suggested that the cells derived from subject 2 are more inducible, whereas cells derived from subject 1 may represent the classical brown fat cells, which possess a very high basal level of UCP1. The distinction of classical versus inducible hBAs between subjects 1 and 2 was further supported by the differential expression levels of the classical BAT marker *ZIC1* (refs. 4,30,31) (**Supplementary Fig. 5g**).

These data support the previous characterization of the tissue from human neck BAT and WAT[20] and demonstrate that the progenitor cell populations we have generated recapitulate adipogenic differentiation and thermogenic expression profiles *in vitro*. Further, inter-subject differences not only exist in whole adipose tissue as previously noted[20], but also exist in adipose progenitors and their derived adipocytes in culture. Despite the inter-subject variations, human brown adipocytes clearly possess high levels of UCP1 and great bioenergetic capacity.

Reporter system for monitoring UCP1 expression

To allow direct assessment of the thermogenic potential of differentiated cells, we introduced a transgenic reporter construct into the white and brown fat precursors to measure *UCP1* gene expression by coupling a bicistronic luciferase and green fluorescent protein (GFP) reporter system to a 4.1-kb human *UCP1* promoter fragment (**Fig. 2a**). In mature adipocytes that stably expressed the reporter construct, luciferase activity was strongly correlated with endogenous *UCP1* gene expression and only detected in mature brown adipocytes, but not in undifferentiated cells (**Fig. 2b**). We monitored differentiating cells using time-lapse microscopy and could detect activation of the GFP reporter as early as day 9 in differentiating BAT cells (**Fig. 2c**

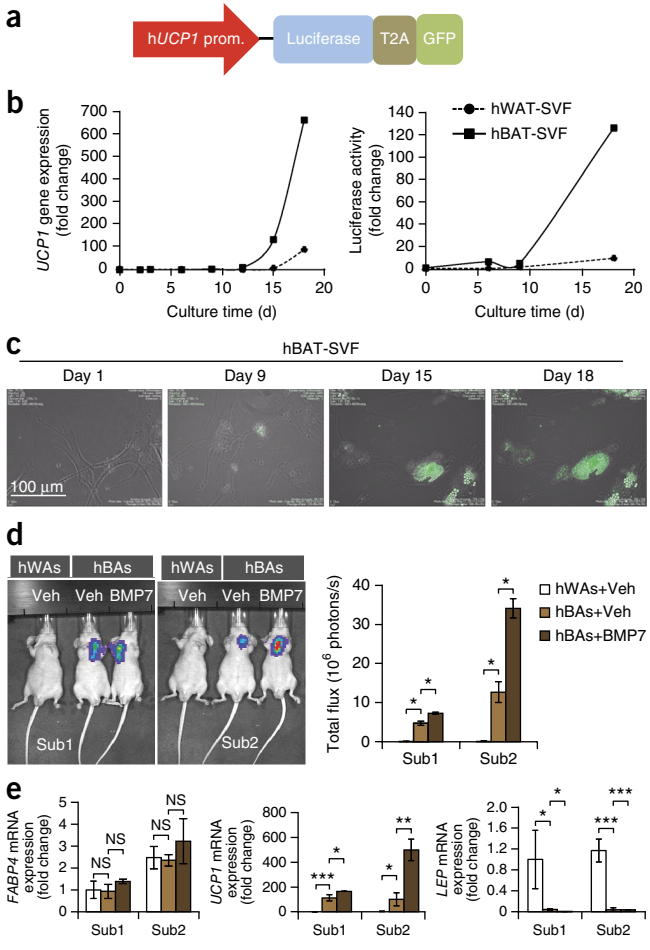

Figure 2 Use of a UCP1 reporter system for *in vitro* and *in vivo* monitoring of UCP1 expression. (**a**) Schematic structure of the h*UCP1* promoter reporter system. 4,148 bp of human *UCP1* promoter drives the expression of bicistronic luciferase and GFP. T2A is the internal ribosomal entry site. (**b**) In hBAT-SVF and hWAT-SVF cells stably expressing the reporter construct, luciferase activity (right) strongly correlated with endogenous *UCP1* gene expression (left) during the course of differentiation (see **Fig. 1a** and Online Methods). Data are presented as fold changes compared to hWAT-SVF cells on day 0 (mean ± s.e.m., $n = 3$ per group, biological replicates). A representative experiment from a total of two independent studies is shown. (**c**) Monitoring *UCP1* expression by GFP *in vitro* using a time-lapse imaging system during differentiation of hBAT-SVF cells from subject 1 (Sub1). (**d**) Left, representative bioluminescent images of nude mice captured 22 d after transplantation of hWAT-SVF and hBAT-SVF cells described in **b**. Right, quantification of luciferase activity by total flux measured in millions of photons per second (error bars are mean ± s.e.m.). The experiments have been repeated twice ($n = 2$ for the hWAT-SVF group; $n = 3$ for the hBAT-SVF group). (**e**) qRT-PCR analysis for expression of *FABP4*, *UCP1* and *LEP* in fat pads developed from the transplanted cells. Data are presented as fold changes compared to fat pads developed from hWAT-SVF cells with vehicle treatment (mean ± s.e.m.). $^{*}P < 0.05$, $^{**}P < 0.01$, $^{***}P < 0.001$ by two-tailed Student's *t*-test. A representative experiment from a total of two independent studies is shown.

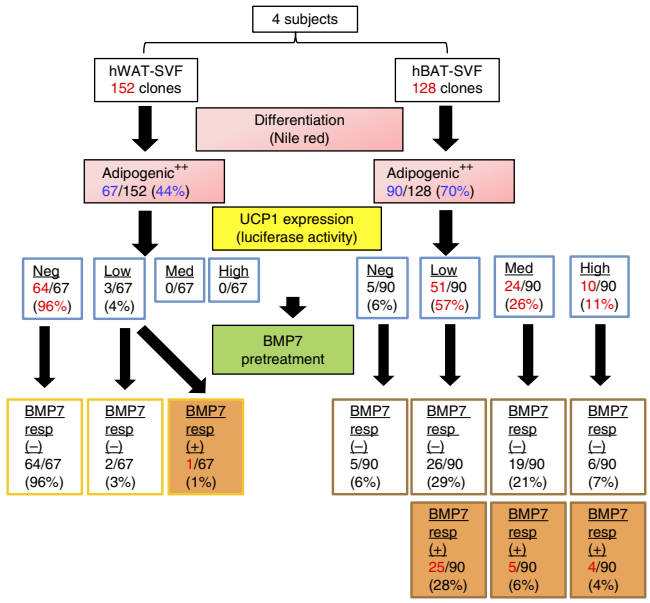

Figure 3 Clonal analysis of human brown and white fat progenitors. The clonal analysis strategy of hWAT-SVF and hBAT-SVF cell progenitors is shown as a dendrogram. 152 clones from hWAT-SVF cells and 128 clones from hBAT-SVF cells were derived by limiting dilution of pooled cells from four subjects. Adipogenic capacity was determined by Nile red staining and *UCP1* levels were determined by luciferase activity on day 18. Detailed selection criteria are described in **Supplementary Figures 6** and **7**. Selected highly adipogenic clones (adipogenic^{++}) were pretreated with 3.3 nM BMP7 for 6 d and then differentiated into mature adipocytes in a 96-well plate. Luciferase activity was measured on day 18 and the cells were divided into different groups on the basis of the level (negative, neg; low; medium, med; and high) of normalized (to protein content) luciferase activity. The positive response (resp. (+)) to BMP7 pretreatment was defined as >1.5-fold increase of luciferase activity in BMP7-pretreated versus vehicle groups.

and **Supplementary Video**). To determine if these cells were capable of differentiation *in vivo*, we transplanted progenitor cells into immune-deficient nude mice and used *in vivo* bioluminescence imaging to measure UCP1 reporter activity. Luciferase activity was high in mice implanted with hBAT progenitors, and it could be further induced by BMP7 pretreatment of progenitors (**Fig. 2d**). Conversely, mice receiving transplanted hWAT progenitors displayed almost no detectable luciferase activity. Although both grafts expressed similar levels of *FABP4*, fat grafts with hBAT-SVF cells displayed at least a 100-fold increase in *UCP1* mRNA compared to hWAT-SVF–derived fat pads, which is consistent with the observed luciferase activity. *LEP* was selectively expressed in fat grafts from hWAT-SVF cells (**Fig. 2e**). These data demonstrate that the UCP1 reporter system accurately indicates differentiation into mature brown adipocytes in both *in vivo* and *in vitro* settings.

Clonal analysis of human brown and white fat progenitors

To study homogenous cell populations derived from human adipose precursor cells, we isolated a total of 280 clonal preadipocyte cell lines (152 hWAT-SVF clones and 128 hBAT-SVF clones) from the pooled immortalized preadipocyte populations from all four subjects. Of these lines, 44% (67 out of 152) of hWAT-SVF and 70% –(90 out of 128) of hBAT-SVF clones robustly differentiated into mature adipocytes (**Fig. 3** and **Supplementary Fig. 6**). To determine *UCP1* induction in the differentiated state, we measured luciferase reporter activity in each clonal line after 18 d of adipogenic differentiation (**Supplementary Fig. 7**). Notably, the data revealed that up to 96% of the hWAT-SVF clones were UCP1 negative, whereas more than 94% of the hBAT-SVF clones displayed different levels of UCP1-luciferase activity (**Fig. 3**).

As shown in **Figure 1h**, certain subpopulations of hWAT or hBAT precursors could respond to inductive signals, such as BMP7, to further increase their thermogenic capacity. To identify the precursor clones that could respond to stimulation, we pretreated undifferentiated cells with BMP7 and determined reporter expression in mature cells. Although only 1% of the highly adipogenic hWAT-SVF clones could respond to BMP7 pretreatment, a substantial number of hBAT-SVF clones (up to 37%) could be induced by BMP7 pretreatment (**Fig. 3**). Further analysis of the clones in terms of their human-subject origins revealed that more than 60% of the hBAT-SVF clones from subjects 2 and 3 could respond to BMP7 stimulation while the majority of the hBAT-SVF clones from subjects 1 and 4 were not responsive to BMP7 pretreatment (**Supplementary Table 2**). These data not only supported the analysis of the pooled progenitor populations described above, but also suggested that the thermogenic features of mature adipocytes are regulated by the anatomical location of the tissue they originate from in addition to genetic influences of the individual human subjects. They also highlighted the heterogeneity of the human adipose clones, even among cell lines isolated from the same subject and a common tissue.

Gene signatures predict thermogenic potential of adipocytes

We aimed to identify molecular markers of thermogenically competent cells. To this end, we took advantage of the UCP1 reporter system for each clonal cell line to select a set of clones from all four subjects, which represented a wide range of luciferase activities after adipogenic differentiation, for further analysis (**Fig. 4a**). We assayed these clones' gene expression profiles in the preadipocyte state using microarrays and correlated these with *UCP1* expression in the differentiated state. After applying the stringent threshold of $P < 0.001$, which is associated with a false discovery rate (FDR) of 0.03, we prioritized 581 genes that displayed significant positive correlation and 454 genes that displayed significant negative correlation (**Fig. 4b**). A subset of these genes is shown along with *UCP1* in **Figure 4c**, illustrating the association between gene expression in the preadipocyte state and *UCP1* expression in the differentiated state. Interestingly, several previously identified brown and white fat markers are among the list of positive or negative predictors (**Supplementary Table 3**).

Scatter plot analysis revealed two general categories of genes in preadipocytes that may regulate induction of a thermogenic program during late stages of differentiation (**Fig. 4d**). The first category of genes could act as binary 'on-and-off' switches to determine cell fate. Positive regulators in this category are likely to be required for thermogenic differentiation, whereas negative regulators would be completely suppressed to allow the *UCP1* gene to be expressed. Representatives of this category included phosphatidylinositol-3,4,5-trisphosphate–dependent Rac exchange factor 1 (*PREX1*)[32], cortactin binding protein 2 (*CTTNBP2*)[33], cardiac actin 1(*ACTC1*)[34] and somatostatin receptor 1 (*SSTR1*)[35]. The second category of genes could act as genetic rheostats to suppress or enhance thermogenic capacity incrementally as their expression levels change. Positive regulators in this category, such as doublesex and mab-3–related transcription factor–like family A1 (*DMRTA1*)[36] and endothelin receptor type B (*EDNRB*)[37], might support thermogenic differentiation in proportion to their expression levels. Negative regulators—such as FAT atypical cadherin 1 (*FAT1*)[38] and protein tyrosine phosphatase, receptor type,

B (*PTPRB*)[39]—might further suppress thermogenic potential when they are more highly expressed. Notably, most of these candidate genes have never been directly implicated in adipocyte differentiation or thermogenic regulation.

Essential roles of *PREX1* and *EDNRB* in thermogenic competency

To select promising candidate genes for further analyses, we applied the following three criteria to the above analysis. First, the primary selection criterion was based on their correlation coefficients,

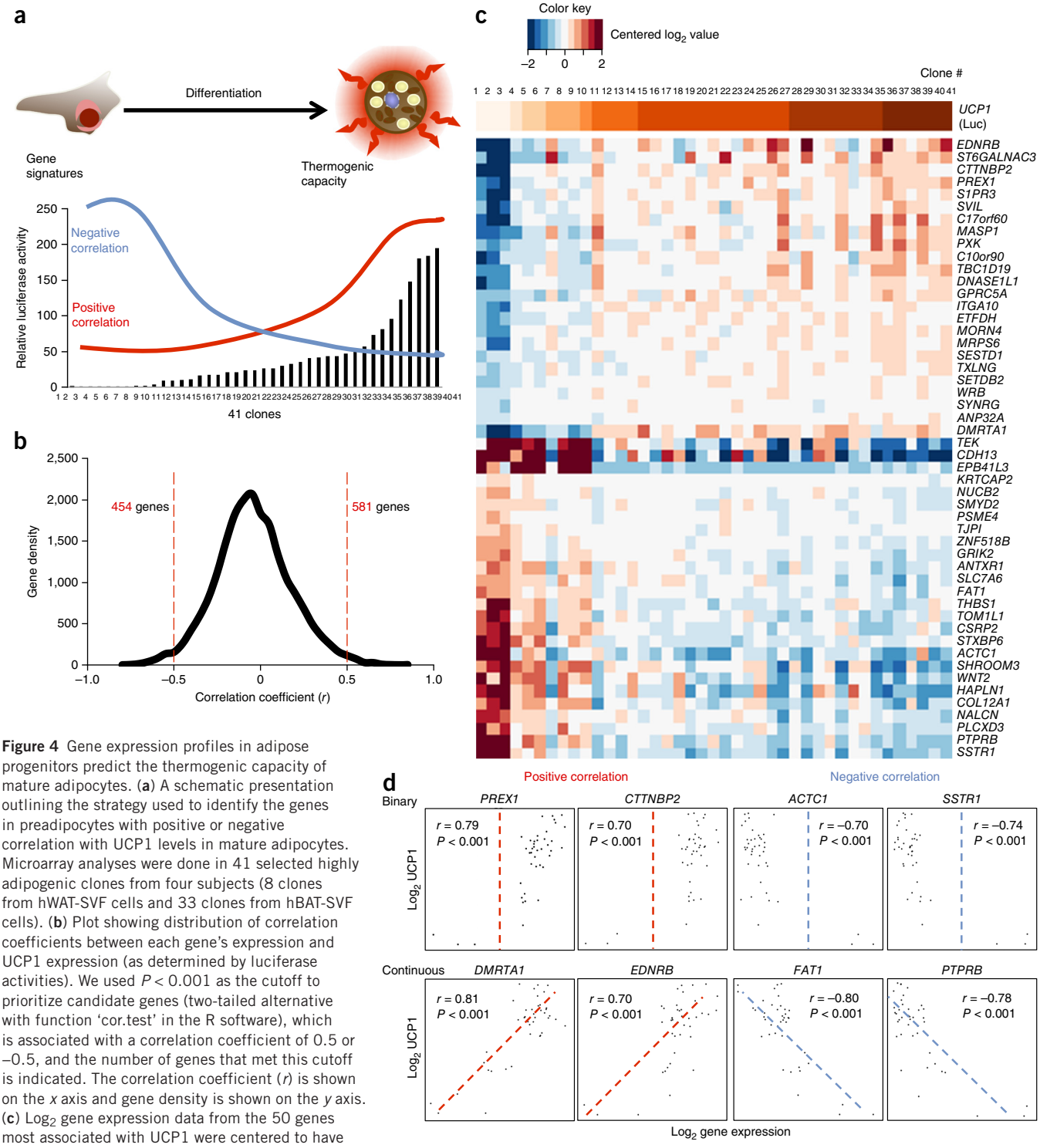

Figure 4 Gene expression profiles in adipose progenitors predict the thermogenic capacity of mature adipocytes. (**a**) A schematic presentation outlining the strategy used to identify the genes in preadipocytes with positive or negative correlation with UCP1 levels in mature adipocytes. Microarray analyses were done in 41 selected highly adipogenic clones from four subjects (8 clones from hWAT-SVF cells and 33 clones from hBAT-SVF cells). (**b**) Plot showing distribution of correlation coefficients between each gene's expression and UCP1 expression (as determined by luciferase activities). We used $P < 0.001$ as the cutoff to prioritize candidate genes (two-tailed alternative with function 'cor.test' in the R software), which is associated with a correlation coefficient of 0.5 or –0.5, and the number of genes that met this cutoff is indicated. The correlation coefficient (r) is shown on the x axis and gene density is shown on the y axis. (**c**) Log_2 gene expression data from the 50 genes most associated with UCP1 were centered to have a mean of zero and restricted to the interval [–2,2] and are shown in a heatmap, along with a color bar representing UCP1 at the top, in which darker indicates higher UCP1 levels (as determined by luciferase activities in the reporter clones). Detailed information of genes is shown in **Supplementary Table 4**. (**d**) Scatter plots showing the positive and negative correlations between the UCP1-luciferase levels and expression levels of candidate genes from microarrays. The log_2 gene expression levels from progenitor cells (day 0) are shown on the x axis. The y axis represents the log_2 UCP1-luciferase levels from mature adipocytes (day 18).

P values and FDR values (**Fig. 4c** and **Supplementary Table 4**). Second, the top-ranking candidate genes were further verified by qRT-PCR assays in a set of ten independent single-cell clones derived from the same four subjects (but not included in the original microarray analysis) for positive or negative correlations between the expression levels of the selected candidate genes in the preadipocytes and *UCP1* mRNA levels in mature adipocytes (**Fig. 5a**). Third, they were also validated in seven pairs of the human neck BAT and WAT (**Supplementary Fig. 8**).

To validate the roles of some of these identified biomarkers in thermogenic capacity, we used CRISPR-Cas9 to knock out the positive *UCP1* regulators *PREX1* and *EDNRB* in an hBAT-SVF clone (**Fig. 5b**). Compared to control cells, gene ablation had no effect on the differentiation of precursor cells into lipid-laden adipocytes that expressed normal levels of *PPARG* (**Fig. 5c**,**d**). Expression of the thermogenic markers *UCP1*, *DIO2* and *PPARGC1A*, however, were markedly decreased in both knockout cell lines (**Fig. 5d**). Consequently, basal respiration, proton leak, and maximal respiration capacity were significantly reduced in *PREX1*-knockout cells compared to control cells ($P = 0.03835$, 0.02884, and 0.00932, respectively) (**Supplementary Fig. 9a–c**). Similarly, *EDNRB*-knockout cells showed a significant reduction of maximal respiration ($P = 0.03351$) and a trend of lower levels of basal respiration and proton leak compared to control cells. To test the effects of a negative regulator on UCP1 expression, we knocked out *SSTR1* in an hWAT-SVF clone (**Fig. 5e**). As we observed for the positive regulators, gene deletion had no effect on adipogenic differentiation, yet thermogenic gene expression remained repressed in white adipocytes (**Fig. 5f**,**g**). These data demonstrated the predictive value of the genes that we identified with our microarray analysis and suggested that the gene expression network that positively regulates thermogenic competency may be more sensitive to perturbation when there is at least some redundancy in the negative regulatory network of genes.

Isolation of thermogenically competent progenitors by CD29

To identify surface markers that could be used to isolate precursors with thermogenic competency, we focused on genes encoding cell surface proteins that had expression patterns that were positively correlated with UCP1 reporter activity (**Fig. 4**). Two members of the integrin family, *ITGA10* (encoding integrin α10) ($P < 0.001$) and *ITGB1* (also known as *CD29*, which encodes integrin β1) ($P < 0.001$), exhibited significantly positive correlations with UCP1 levels (**Fig. 6a**,**b**). Integrins are heterodimeric transmembrane receptors that mediate various biological functions, such as cell proliferation, differentiation, and migration[40,41]. Using FACS with an antibody specific to CD29, we were able to separate subpopulations of cells from pooled hWAT-SVF and pooled hBAT-SVF cells on the basis of

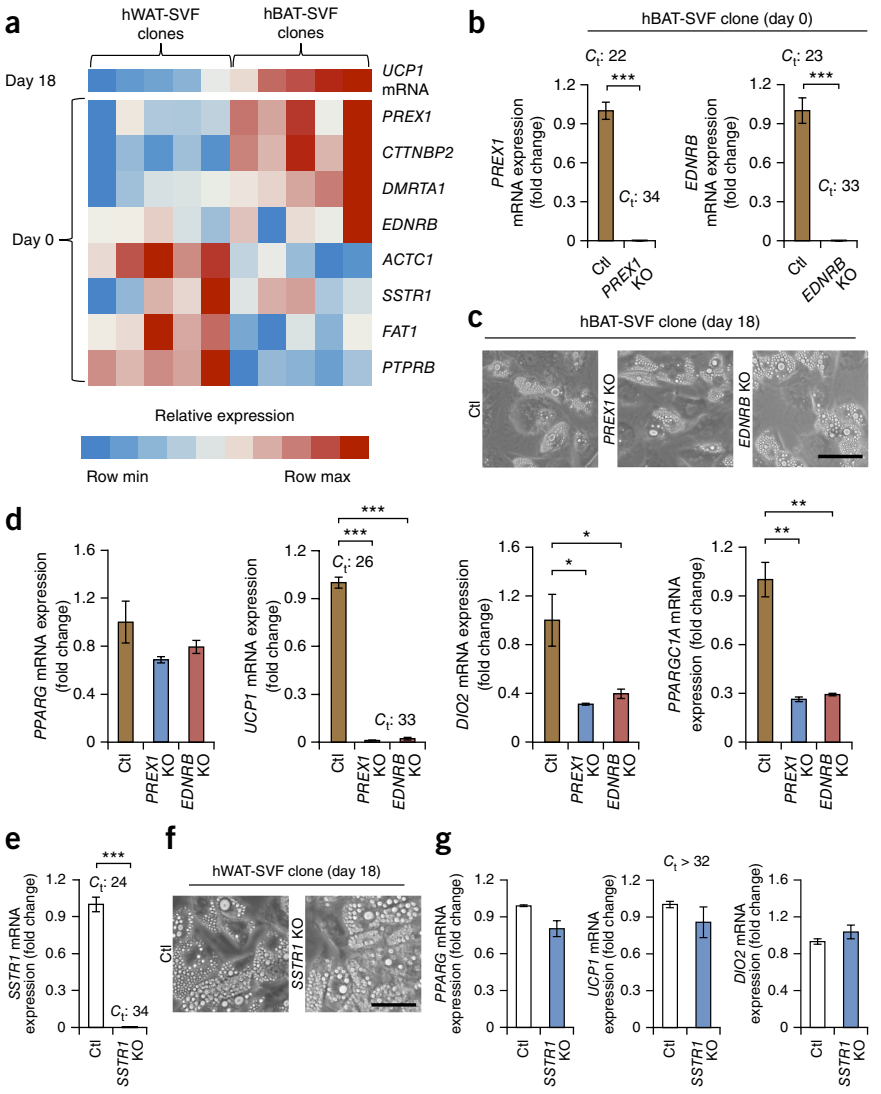

Figure 5 *PREX1* and *EDNRB* are required for determining thermogenic competency. (**a**) Heatmap displaying correlations between *UCP1* mRNA levels on day 18 (top row) and expression levels of candidate genes on day 0. Data were obtained from 10 independent hWAT-SVF and hBAT-SVF clones derived from the same four subjects that were not included in microarray analyses. Values were normalized within each row using a linear color scale. (**b**) mRNA levels of *PREX1* and *EDNRB* were measured by qRT-PCR in *PREX1*- and *EDNRB*-knockout (KO) hBAT-SVF clones made using CRISPR-Cas9 technology. The results were verified in another progenitor clone. (**c**) Microscopic views of differentiated *PREX1*-KO and *EDNRB*-KO hBAT-SVF cells. Ctl, control cells. Scale bar, 100 µm. (**d**) qRT-PCR analysis for *PPARG* and brown fat–specific markers (*UCP1*, *DIO2* and *PPARGC1A*) in differentiated *PREX1*-KO and *EDNRB*-KO hBAT-SVF cells. (**e**) *SSTR1* level was detected by qRT-PCR in a *SSTR1*-KO hWAT-SVF clone that was made using CRISPR-Cas9. The results were verified in another progenitor clone. (**f**) Bright-field images of a differentiated *SSTR1*-KO hWAT-SVF clone. Scale bar, 100 µm. (**g**) qRT-PCR analysis for *PPARG* and brown fat–specific markers (*UCP1* and *DIO2*) from a differentiated *SSTR1*-KO clone. qRT-PCR data are presented as fold change compared to control cells (Ctl) (mean ± s.e.m., $n = 3$ per group, biological replicates; two-tailed Student's *t*-test; $^{*}P < 0.05$, $^{**}P < 0.01$, $^{***}P < 0.001$). The C_t values are indicated to reflect the actual gene expression levels.

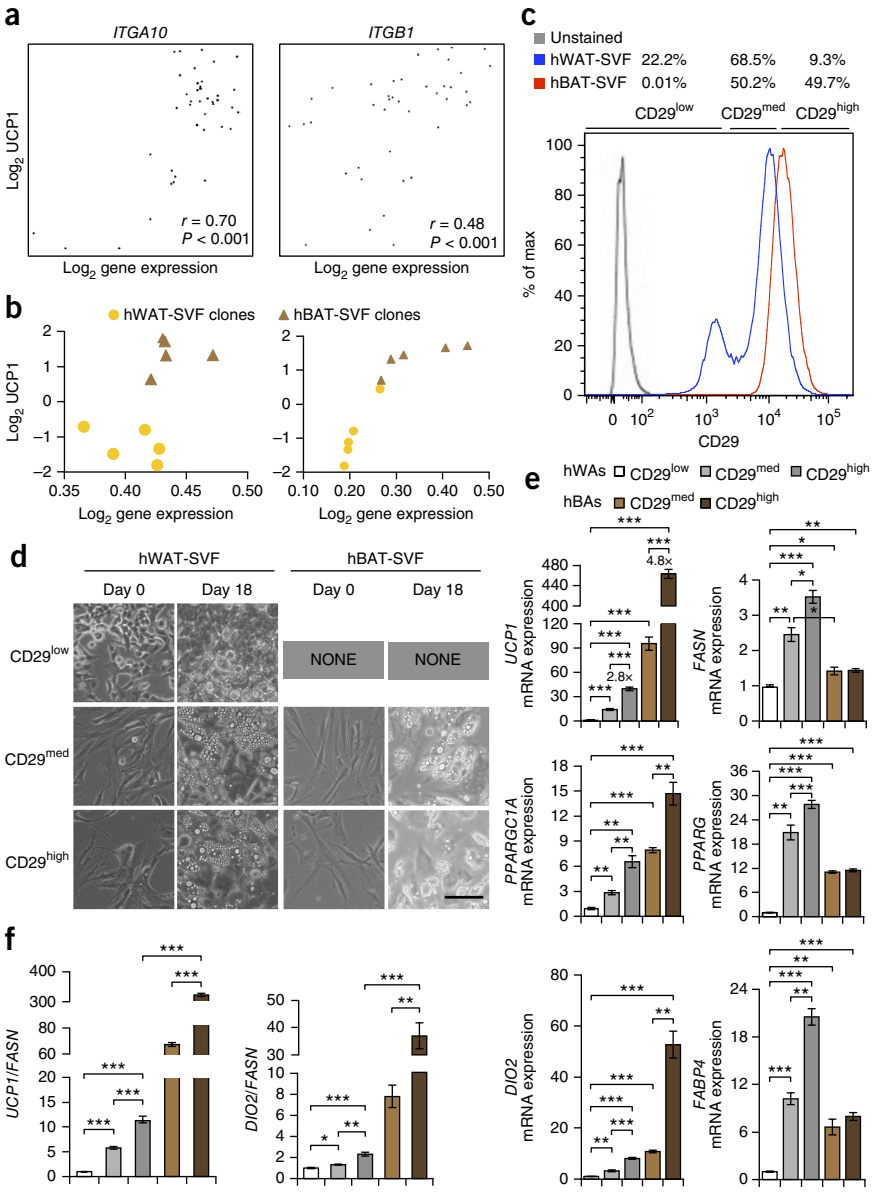

Figure 6 Isolation of progenitors possessing thermogenic potential using a cell surface marker. (**a**) Scatter plots showing positive correlation between the UCP1-luciferase levels (shown as $\log_2$ levels on the *y* axis) on day 18 and expression levels of *ITGA10* (left) and *ITGB1* (right) (shown as $\log_2$ levels on the *x* axis) on day 0 from microarray analyses. (**b**) Correlation between the mRNA levels of *ITGA10* and *ITGB1* (shown as $\log_2$ levels on the *x* axis) on day 0 and *UCP1* mRNA levels (shown as $\log_2$ levels on the *y* axis) on day 18 in ten independent hWAT-SVF and hBAT-SVF clones, as described in **Figure 5a**. (**c**) Histogram displaying subpopulations with differential levels of CD29 from pooled hWAT-SVF (blue) and hBAT-SVF (red) cells using FACS. Gray line represents unstained cells. (**d**) Images of sorted subpopulations with different levels of CD29 ($CD29^{low}$, $CD29^{med}$ and $CD29^{high}$) on days 0 and 18 are shown. Note that we could not sort enough numbers of $CD29^{low}$ cells from pooled hBAT-SVF cells, and thus results from this subpopulation are not shown. Scale bar, 100 µm. A representative experiment from two independent studies is shown. (**e**) qRT-PCR analysis for the adipocyte markers (*FASN*, *PPARG* and *FABP4*) and brown fat–specific markers (*UCP1*, *PPARGC1A* and *DIO2*) on the indicated differentiated populations. (**f**) To correct for the different degrees of adipogenesis shown in **e**, expression levels of *UCP1* and *DIO2* were normalized to the level of the mature adipocyte marker, *FASN*. Data are presented as mean ± s.e.m. ($n = 3$ per group, biological replicates; two-tailed Student's *t*-test; $^*P < 0.05$, $^{**}P < 0.01$, $^{***}P < 0.001$).

the abundance of CD29 on the cell surface. We noted that the hWAT-SVF population contained 22.2% $CD29^{low}$, 68.5% $CD29^{med}$ and 9.3% $CD29^{high}$ cells, whereas the hBAT-SVF population had almost equal proportions of $CD29^{med}$ and $CD29^{high}$ cells (50.2% and 49.7%, respectively) and very few $CD29^{low}$ cells (0.01%) (**Fig. 6c**). The ability of $CD29^+$ hWAT-SVF cells to differentiate into lipid-laden cells appeared to positively correlate with CD29 levels (**Fig. 6d**). Notably, $CD29^{high}$ hBAT-SVF cells effectively differentiated into brown adipocytes that expressed the highest levels of *UCP1* among all the groups (**Fig. 6e**,**f**). These data suggested the exciting potential of using an antibody against CD29 to prospectively isolate human adipose progenitors that could give rise to mature adipocytes with great thermogenic capability.

DISCUSSION

In this study we generated cell lines that served as models to tease apart the heterogeneity of human BAT and WAT; this will, in turn, allow further investigations into the functions of these types of cells. The cell lines we generated robustly differentiated into cells and tissue that recapitulated the gene expression signature and metabolic capacity of BAT. Interestingly, differentiated hBAs displayed greater ability in glucose and fatty acid uptake, and fatty acid oxidation, compared to differentiated hWAs, indicating that human brown adipocytes are capable of using both glucose and fatty acids as fuels. In addition, we have generated cell lines stably expressing a UCP1 reporter construct. By allowing the longitudinal measurement of UCP1 reporter activity, these cells offer great opportunities for high-throughput screens aimed at identifying targets that enhance thermogenic differentiation or activate mature cells. Furthermore, the UCP1 reporter allows for the generation of human xenograft models wherein human BAT and WAT can be dynamically assayed for induction of UCP1 *in vivo*. Our proof-of-concept experiment using BMP7 pretreatment of hBAT preadipocytes demonstrates the exciting prospect of using mice with human-derived BAT and WAT to screen for novel activators of thermogenesis in an *in vivo* setting.

Microarray analysis in adipose clones revealed two general classifications of genes that regulate thermogenic differentiation: the binary 'on-and-off' category and the continuous category. These two categories of genes suggest a distinct commitment step in brown adipogenesis, which is followed by differentiation. Both categories of genes present interesting opportunities for modulating cellular energy balance. By activating 'on' switches and deactivating 'off' switches, it may be possible to activate pools of precursor cells to differentiate

into brown adipocytes. This approach may need to be combined with a second strategy targeting the genes that act as genetic rheostats with the goal of fine-tuning the regulators to increase UCP1 expression in adipocytes.

Indeed, by using CRISPR-Cas9 to knock out the positive UCP1 regulators *PREX1* and *EDNRB* in brown preadipocytes, we could almost completely abolish the high levels of UCP1 in mature brown fat cells. However, ablation of the negative regulator *SSTR1* in white fat precursors failed to turn on the thermogenic program. These findings suggest that these positive regulators have an essential role in determining thermogenic competency in brown preadipocytes. By contrast, it may take a combined approach to remove multiple negative regulators—and perhaps turn on positive modulators—in the human white preadipocytes in order to activate their thermogenic program.

PREX1 is a guanine-nucleotide exchange factor for the Rho small GTP-binding proteins. It has been shown to promote glucose transporter type 4 (Glut4) trafficking in 3T3-L1 adipocytes[42], and single-nucleotide polymorphisms near *PREX1* are linked to susceptibility to type 2 diabetes through *PREX1*'s potential effect on adiposity[43]. Endothelin, the ligand of EDNRB, can modulate intracellular calcium and cAMP levels, stimulate glucose uptake and activate lipolysis in adipocytes[44,45]. Thus, it is possible that *PREX1* and *EDNRB* might regulate pathways controlling fuel use in preadipocytes, which poise the cells to become thermogenically competent in mature adipocytes. The role of these markers in human obesity warrants future investigation.

Recently, Shinoda *et al.*[46] identified two human BAT markers, *KCNK3* and *MTUS1*. Of note, although the expression of these genes in our preadipocyte clones does not show significant correlation with UCP1 expression in adipocytes (**Supplementary Table 3**), they are indeed more highly expressed in the differentiated hBAs than in hWAs (**Supplementary Fig. 9e**). Given the differences in the anatomical locations from which these cells are derived and the approaches used in these two studies, it is conceivable that distinct markers would be identified. Additionally, these findings actually complement each other because the markers identified by Shinoda *et al.*[46] serve as mature hBAT markers, whereas gene signatures identified in the current study represent markers in human preadipocytes that are predictive of thermogenic capacity in mature adipocytes.

Single-cell clonal analysis revealed a large number of clones that could differentiate and accurately recapitulate BAT and WAT behavior. Notably, although these cells represented a broad range of thermogenic competencies, they demonstrated a consistent increase in thermogenic capacity in BAT cells compared to WAT cells. However, the influence of each subject's characteristics was still apparent. These characteristics included genetic background, sex, and body mass index, as well as the anatomic locations from which the fat depots were collected. These factors may contribute to the differential responses to stimuli that cause preadipocytes to become thermogenically active cells upon stimulation, and this needs to be further investigated by generating and characterizing adipose precursors from additional individuals of representative populations.

Here we have shown the utility of a CD29-specific antibody to prospectively isolate human preadipocytes with high thermogenic potential, and we suggest the prospect of using this approach to assess the thermogenic potential of different patient populations. $CD29^+$ cells from adipose tissue possess great adipogenic differentiation potential[47]. Our data also showed a similar result wherein the degree of lipid accumulation positively correlated with the levels of CD29 in hWAT-SVF cells. CD29 is involved in the formation of the transmembrane linkage between the extracellular matrix and the microfilaments[48,49], suggesting that the regulatory events that affect cell adhesion and cell shape during adipocyte differentiation might have a role in determining thermogenic potential.

An understanding of the cellular identity of human adipose tissue is key to formulating therapeutic interventions to treat obesity and its sequelae. The cell-based models reported here not only provide a promising opportunity to study adipogenesis and the gene patterns that regulate thermogenic competency, but also offer potential avenues for developing effective therapies for treating obesity and its many associated metabolic diseases.

METHODS

Methods and any associated references are available in the online version of the paper.

Accession codes. Gene Expression Omnibus (GEO) repository: microarray data have been deposited with accession number GSE68544.

Note: Any Supplementary Information and Source Data files are available in the online version of the paper.

ACKNOWLEDGMENTS

This work was supported in part by US National Institutes of Health (NIH) grants R01DK077097 (to Y.-H.T.), R01DK099511 (to L.J.G.), K23DK081604 (to A.M.C.) and P30DK036836 (to Joslin Diabetes Center's Diabetes Research Center, DRC) from the National Institute of Diabetes and Digestive and Kidney Diseases, a sponsored research grant from Chugai Pharmaceutical Co. (to Y.-H.T. and A.M.C.), a research grant from the American Diabetes Association (ADA 7-12-BS-191, to Y.-H.T.), the Intramural Research Program of the National Institute of Diabetes and Digestive and Kidney Diseases (NIDDK), and by funding from the Harvard Stem Cell Institute (to Y.-H.T.). M.D.L. was supported by NIH fellowships (T32DK007260 and F32DK102320). We thank M.-E. Patti and K. Hughes of the Advanced Genomics and Genetics Core of Joslin's DRC for advice and expert technical assistance. The authors thank Stryker Regenerative Medicine (Hopkinton, Massachusetts) for the generous gift of recombinant BMP7.

AUTHOR CONTRIBUTIONS

The study was designed by Y.-H.T., R.X., M.D.L. and A.M.C. The manuscript was written by Y.-H.T., M.D.L., R.X. and J.M.D. R.X. performed the majority of the experiments. M.D.L. did the time-lapse imaging, IVIS scanning and FACS. J.M.D. analyzed microarray data. F.S. performed bioenergetics analyses in knockout cells. T.J.S. and H.Z. established the method of isolation, immortalization and differentiation of human fat progenitors. T.L.H. did the human cell implantation and gene expression microarrays. K.L.T. provided assistance with the Seahorse bioanalyzer. Y.L. provided research assistance. H.T. and L.J.G. helped with fuel utilization experiments. A.M.C., L.S.W. and A.P.W. collected human fat samples. M.S.L. and L.L.R. helped with the time-lapse imaging. All authors contributed to editing the manuscript.

COMPETING FINANCIAL INTERESTS

The authors declare competing financial interests; details are available in the online version of the paper.

1. Cannon, B. & Nedergaard, J. Brown adipose tissue: function and physiological significance. *Physiol. Rev.* **84**, 277–359 (2004).
2. Schulz, T.J. & Tseng, Y.H. Brown adipose tissue: development, metabolism and beyond. *Biochem. J.* **453**, 167–178 (2013).
3. Guerra, C., Koza, R.A., Yamashita, H., Walsh, K. & Kozak, L.P. Emergence of brown adipocytes in white fat in mice is under genetic control. Effects on body weight and adiposity. *J. Clin. Invest.* **102**, 412–420 (1998).
4. Petrovic, N. *et al.* Chronic peroxisome proliferator-activated receptor gamma (PPARγ) activation of epididymally derived white adipocyte cultures reveals a population of thermogenically competent, UCP1-containing adipocytes molecularly distinct from classic brown adipocytes. *J. Biol. Chem.* **285**, 7153–7164 (2010).
5. Harms, M. & Seale, P. Brown and beige fat: development, function and therapeutic potential. *Nat. Med.* **19**, 1252–1263 (2013).
6. Nedergaard, J. & Cannon, B. The browning of white adipose tissue: some burning issues. *Cell Metab.* **20**, 396–407 (2014).

7. Bartelt, A. *et al.* Brown adipose tissue activity controls triglyceride clearance. *Nat. Med.* **17**, 200–205 (2011).
8. Stanford, K.I. *et al.* Brown adipose tissue regulates glucose homeostasis and insulin sensitivity. *J. Clin. Invest.* **123**, 215–223 (2013).
9. Nedergaard, J., Bengtsson, T. & Cannon, B. Unexpected evidence for active brown adipose tissue in adult humans. *Am. J. Physiol. Endocrinol. Metab.* **293**, E444–E452 (2007).
10. Cypess, A.M. *et al.* Identification and importance of brown adipose tissue in adult humans. *N. Engl. J. Med.* **360**, 1509–1517 (2009).
11. van Marken Lichtenbelt, W.D. *et al.* Cold-activated brown adipose tissue in healthy men. *N. Engl. J. Med.* **360**, 1500–1508 (2009).
12. Virtanen, K.A. *et al.* Functional brown adipose tissue in healthy adults. *N. Engl. J. Med.* **360**, 1518–1525 (2009).
13. Saito, M. *et al.* High incidence of metabolically active brown adipose tissue in healthy adult humans: effects of cold exposure and adiposity. *Diabetes* **58**, 1526–1531 (2009).
14. Zingaretti, M.C. *et al.* The presence of UCP1 demonstrates that metabolically active adipose tissue in the neck of adult humans truly represents brown adipose tissue. *FASEB J.* **23**, 3113–3120 (2009).
15. Himms-Hagen, J. *et al.* Effect of CL-316,243, a thermogenic β3-agonist, on energy balance and brown and white adipose tissues in rats. *Am. J. Physiol.* **266**, R1371–R1382 (1994).
16. Yoneshiro, T. *et al.* Recruited brown adipose tissue as an antiobesity agent in humans. *J. Clin. Invest.* **123**, 3404–3408 (2013).
17. van der Lans, A.A. *et al.* Cold acclimation recruits human brown fat and increases nonshivering thermogenesis. *J. Clin. Invest.* **123**, 3395–3403 (2013).
18. Ouellet, V. *et al.* Brown adipose tissue oxidative metabolism contributes to energy expenditure during acute cold exposure in humans. *J. Clin. Invest.* **122**, 545–552 (2012).
19. Wu, J. *et al.* Beige adipocytes are a distinct type of thermogenic fat cell in mouse and human. *Cell* **150**, 366–376 (2012).
20. Cypess, A.M. *et al.* Anatomical localization, gene expression profiling and functional characterization of adult human neck brown fat. *Nat. Med.* **19**, 635–639 (2013).
21. Lidell, M.E. *et al.* Evidence for two types of brown adipose tissue in humans. *Nat. Med.* **19**, 631–634 (2013).
22. Jespersen, N.Z. *et al.* A classical brown adipose tissue mRNA signature partly overlaps with brite in the supraclavicular region of adult humans. *Cell Metab.* **17**, 798–805 (2013).
23. Schulz, T.J. *et al.* Identification of inducible brown adipocyte progenitors residing in skeletal muscle and white fat. *Proc. Natl. Acad. Sci. USA* **108**, 143–148 (2011).
24. Lee, Y.H., Petkova, A.P., Mottillo, E.P. & Granneman, J.G. *In vivo* identification of bipotential adipocyte progenitors recruited by β3-adrenoceptor activation and high-fat feeding. *Cell Metab.* **15**, 480–491 (2012).
25. Berry, R. & Rodeheffer, M.S. Characterization of the adipocyte cellular lineage *in vivo*. *Nat. Cell Biol.* **15**, 302–308 (2013).
26. Wang, W. *et al.* Ebf2 is a selective marker of brown and beige adipogenic precursor cells. *Proc. Natl. Acad. Sci. USA* **111**, 14466–14471 (2014).
27. Tchkonia, T. *et al.* Fat depot–specific characteristics are retained in strains derived from single human preadipocytes. *Diabetes* **55**, 2571–2578 (2006).
28. Whittle, A.J. *et al.* BMP8B increases brown adipose tissue thermogenesis through both central and peripheral actions. *Cell* **149**, 871–885 (2012).
29. Tseng, Y.H. *et al.* New role of bone morphogenetic protein 7 in brown adipogenesis and energy expenditure. *Nature* **454**, 1000–1004 (2008).
30. Seale, P. *et al.* Transcriptional control of brown fat determination by PRDM16. *Cell Metab.* **6**, 38–54 (2007).
31. Timmons, J.A. *et al.* Myogenic gene expression signature establishes that brown and white adipocytes originate from distinct cell lineages. *Proc. Natl. Acad. Sci. USA* **104**, 4401–4406 (2007).
32. Welch, H.C. *et al.* P-Rex1, a PtdIns(3,4,5)P3- and Gβγ-regulated guanine-nucleotide exchange factor for Rac. *Cell* **108**, 809–821 (2002).
33. Cheung, J. *et al.* Identification of the human cortactin-binding protein-2 gene from the autism candidate region at 7q31. *Genomics* **78**, 7–11 (2001).
34. Zhang, S.X. *et al.* Identification of direct serum-response factor gene targets during Me_2SO-induced P19 cardiac cell differentiation. *J. Biol. Chem.* **280**, 19115–19126 (2005).
35. Yamada, Y. *et al.* Cloning and functional characterization of a family of human and mouse somatostatin receptors expressed in brain, gastrointestinal tract and kidney. *Proc. Natl. Acad. Sci. USA* **89**, 251–255 (1992).
36. Kikkawa, T. *et al.* Dmrta1 regulates proneural gene expression downstream of Pax6 in the mammalian telencephalon. *Genes Cells* **18**, 636–649 (2013).
37. Garciafigueroa, D.Y., Klei, L.R., Ambrosio, F. & Barchowsky, A. Arsenic-stimulated lipolysis and adipose remodeling is mediated by G-protein–coupled receptors. *Toxicol. Sci.* **134**, 335–344 (2013).
38. Chen, T.Y. *et al.* Endogenous n-3 polyunsaturated fatty acids (PUFAs) mitigate ovariectomy-induced bone loss by attenuating bone marrow adipogenesis in *FAT1* transgenic mice. *Drug Des. Devel. Ther.* **7**, 545–552 (2013).
39. Behjati, S. *et al.* Recurrent *PTPRB* and *PLCG1* mutations in angiosarcoma. *Nat. Genet.* **46**, 376–379 (2014).
40. Takada, Y., Ye, X. & Simon, S. The integrins. *Genome Biol.* **8**, 215 (2007).
41. Margadant, C., Monsuur, H.N., Norman, J.C. & Sonnenberg, A. Mechanisms of integrin activation and trafficking. *Curr. Opin. Cell Biol.* **23**, 607–614 (2011).
42. Balamatsias, D. *et al.* Identification of P-Rex1 as a novel Rac1-guanine nucleotide exchange factor (GEF) that promotes actin remodeling and GLUT4 protein trafficking in adipocytes. *J. Biol. Chem.* **286**, 43229–43240 (2011).
43. Lewis, J.P. *et al.* Analysis of candidate genes on chromosome 20q12–13.1 reveals evidence for BMI-mediated association of *PREX1* with type 2 diabetes in European Americans. *Genomics* **96**, 211–219 (2010).
44. Wu-Wong, J.R., Berg, C.E. & Dayton, B.D. Endothelin-stimulated glucose uptake: effects of intracellular Ca^{2+}, cAMP and glucosamine. *Clin. Sci.* **103** (suppl. 48), 418S–423S (2002).
45. Juan, C.C. *et al.* Effect of endothelin-1 on lipolysis in rat adipocytes. *Obesity (Silver Spring)* **14**, 398–404 (2006).
46. Shinoda, K. *et al.* Genetic and functional characterization of clonally derived adult human brown adipocytes. *Nat. Med.* **21**, 389–394 (2015).
47. Gierloff, M. *et al.* Adipogenic differentiation potential of rat adipose tissue–derived subpopulations of stromal cells. *J. Plast. Reconstr. Aesthet. Surg.* **67**, 1427–1435 (2014).
48. Farnier, C. *et al.* The signaling pathway for β1-integrin/ERKs is involved in the adaptation of adipocyte functions to cell size. *Ann. NY Acad. Sci.* **973**, 594–597 (2002).
49. Kawaguchi, N. *et al.* ADAM12 induces actin cytoskeleton and extracellular matrix reorganization during early adipocyte differentiation by regulating β1 integrin function. *J. Cell Sci.* **116**, 3893–3904 (2003).

ONLINE METHODS

Materials. Recombinant human BMP7 was kindly provided by Stryker Regenerative Medicine (Hopkinton, MA) and recombinant human BMP8 was purchased from R&D Systems (Minneapolis, MN). Antibody sources are as follows: anti-UCP1 was from Abcam (Cambridge, MA, ab155117) and AnaSpec (Fremont, CA, cat. no. 53936); anti-α-tubulin was from Sigma-Aldrich (Dallas, TX, T6074); and anti-CD29 was from eBioscience (San Diego, CA, clone TS2/16). All other chemicals were purchased from Sigma-Aldrich (Dallas, TX), unless otherwise specified.

Human subjects. This study followed the institutional guidelines of and was approved by the Human Studies Institutional Review Boards of Beth Israel Deaconess Medical Center and Joslin Diabetes Center. Details on procedures of human subject collection were described previously[20]. There were two independent human subject cohorts: for isolation and immortalization of fat progenitors, human neck fat from four subjects was analyzed (clinical characteristics of subjects are provided in **Supplementary Table 1a**); for gene expression verification, neck fat from seven different people was studied (clinical characteristics of subjects are provided in **Supplementary Table 1b**). All subjects gave written informed consent before taking part in the study.

Isolation and culture of primary human white and brown fat progenitors. Isolation of primary SVF from human neck fat was described previously[20]. Owing to the limited amount of human brown fat tissue collected from surgeries, we pooled fat depots from the same subject to obtain sufficient numbers of SVF cells for primary culture as well as immortalization. Specifically, subcutaneous and subplatysmal neck fat depots were pooled to generate hWAT-SVF cells and deep neck fat depots collected from the carotid sheath, longus colli muscle and prevertebral regions were combined for generation of hBAT-SVF cells. Freshly resected fat depots were collected, minced and digested using collagenase 1 (2 mg/ml in PBS with the addition of 3.5% BSA; Worthington Biochemical Corporation, Lakewood, NJ), and the SVF was isolated. SVF cells were plated and grown in high-glucose Dulbecco's modified Eagle's medium (DMEM/H) supplemented with 10% (vol/vol) fetal bovine serum (FBS) and 1% penicillin-streptomycin. For adipocyte differentiation, cells were grown to confluence for 6 d (referred to as 'day 6') and then exposed to adipogenic induction mixture in DMEM/H medium containing 0.5 mM isobutylmethylxanthine, 0.1 μM dexamethasone, 0.5 μM human insulin (Sigma-Aldrich, Dallas, TX), 2 nM T3, 30 μM indomethacin, 17 μM pantothenate, 33 μM biotin and 2% FBS for another 12 d (referred to as 'day 18'). Induction medium was changed every 3 d until cells were collected.

Generation of immortalized human brown and white fat progenitors. Primary SVF cells were immortalized with hTERT as described[27]. Primary SVF isolated from four subjects that had undergone four or five population doublings were separately infected with a retrovirus containing the plasmid, pBABE-hTERT-Hygro (Addgene no. 1773, Cambridge, MA), which expresses hTERT driven by a long-terminal-repeat promoter. Phoenix-A cells (ATCC) were transfected with pBABE-hTERT-Hygro DNA using PolyJet DNA *in vitro* transfection reagent (SignaGen Laboratories, Rockville, MD). Culture supernatants containing virus were collected every 24 h after transfection and filtered through a 0.45 μm filter (Fisher Scientific, Pittsburgh, PA). Primary SVF cells from human white and brown fat at 80% confluence were infected with supernatants in the presence of 4 μg/ml Polybrene every day until cells reached 90% confluence. Cells were then treated with hygromycin (concentrations ranging from 100 μg/ml to 400 μg/ml, depending on cell conditions) in DMEM/H medium containing 10% FBS and antibiotics. Once drug selection was finished, the cells were maintained in culture medium with 50 μg/ml hygromycin for 2 weeks.

Culture and differentiation of immortalized human white and brown fat progenitors. Immortalized progenitor cells were plated and grown in DMEM/H medium supplemented with 10% FBS (day 0). For adipocyte differentiation, cell were grown for 6 d until reaching confluence (day 6), and then treated with the adipogenic induction medium as described above for 12 d (day 18). To further stimulate the thermogenic program, fully differentiated cells were incubated with 10 μM forskolin or 1 μM norepinephrine for 4 h. For BMPs and FGF21 pretreatment, recombinant BMP7 (3.3 nM), BMP8 (3.3 nM) or FGF21 (50 nM) were added to undifferentiated cells in medium containing insulin (0.5 μM), T3 (2 nM) and 2% FBS for 6 d followed by adipogenic induction for 12 d. For BMPs and FGF21 post-treatment, fully differentiated adipocytes at day 18 were treated with recombinant BMP7 (3.3 nM), BMP8 (3.3 nM) or FGF21 (50 nM) in medium containing insulin (0.5 μM), T3 (2 nM) and 2% FBS for 2 d. We routinely checked for mycoplasma contamination and all the cells used in this study were free of mycoplasma.

Oil Red O staining. Cells were washed twice with PBS and fixed with 10% buffered formalin for 30 min at room temperature. Cells were then stained for 4 h at room temperature with a filtered Oil Red O solution (0.5% Oil Red O in isopropyl alcohol), washed twice with distilled water, and then visualized.

Quantitative RT-PCR. RNA extraction, cDNA synthesis, and qRT-PCR were performed as described before[20,29]. qRT-PCR assays were run in duplicate and quantified in the ABI Prism 7900 sequence-detection system using SYBR (Roche Applied Science, Indianapolis, IN). Relative mRNA expression was determined by the ΔC_t method and the values were normalized to the expression of 18S ribosomal RNA (18S). The sequences of primers used in this study are provided in **Supplementary Table 5**.

Western blotting. Protein detection by western blotting was performed as described before[29]. Primary antibodies were incubated overnight at 4 °C: UCP1 (1:500, rabbit polyclonal; Abcam, Cambridge, MA) and α-tubulin (1:4,000, mouse monoclonal). HRP-coupled secondary antibodies (Cell Signaling Technologies, Beverly, MA) were used at 1:2,000 dilutions at room temperature for 2 h followed by detection using the Amersham enhanced chemiluminescence (ECL) prime (GE healthcare, Pittsburgh, PA).

Bioenergetic profiling. To assess mitochondrial respiration, a Seahorse Extracellular Flux Analyzer (Seahorse Bioscience Inc., North Billerica, MA) was used to quantify oxygen consumption rates (OCR) of differentiated human white and brown adipocytes. Progenitor cells were seeded on 24-well format plates and allowed to adhere overnight. After 6 d, adipogenesis was induced as described above. After adipogenic induction for 12 d, OCR was analyzed. To measure OCR independent of oxidative phosphorylation, 0.5 μM oligomycin (EMD Chemicals Inc., Gibbstown, NJ) was added to cells. Subsequently, 0.8 μM FCCP (carbonyl cyanide-*p*-trifluoromethoxyphenylhydrazone) and 1 μM respiratory chain inhibitor (rotenone) were added to measure maximal respiration and basal rates of nonmitochondrial respiration. For cAMP-induced respiration, fully differentiated adipocytes were incubated with 10 μM forskolin for 4 h. For BMP7 pretreatment-induced respiration, recombinant BMP7 (3.3 nM) was added to the undifferentiated cells for 6 d and then adipogenic induction mixture medium was added to the confluent cells for 12 d, followed by measurement of cellular respiration. All data were average of four time points with 10 wells per time point quantified in bar plots, and error bars are s.e.m. Statistical comparisons were done by Student's *t*-test.

Glucose uptake assay. After serum starvation in DMEM/H medium containing 1% BSA for 2–3 h, differentiated human white and brown adipocytes were washed with HEPES buffer. Then they were incubated with or without 100 nM insulin for 30 min in DMEM/H medium containing 1% BSA. Glucose transport was determined by the addition of 2-deoxy-[^{3}H]glucose (0.1 mM, 0.5 μCi/ml; PerkinElmer Life and Analytical Science, Waltham, MA). After 5 min of incubation, the reaction was stopped with ice-cold PBS and cells were washed twice in ice-cold PBS. Cells were then lysed in 0.1% SDS, and glucose uptake was assessed in 4 ml of scintillant using a Beckman LS6500 scintillation counter (Beckman Coulter, Indianapolis, IN). Nonspecific 2-deoxy-[^{3}H]glucose uptake was measured in the presence of cytochalasin B (20 μM) and was subtracted from the total uptake to get specific glucose uptake. Results were expressed as the mean ± s.e.m. of the indicated number of experiments. The protein content was determined by the Bradford method.

Fatty acid uptake and fatty acid oxidation assays. Fatty acid uptake and oxidation were determined by measuring both [^{14}C]palmitic acid uptake and

conversion of [^{14}C]palmitic acid into CO_2. Briefly, the culture medium was removed, and cells were incubated with DMEM/H containing 4% fatty acid–free BSA, 0.5 mM palmitic acid, and 0.2 μCi/ml [1-^{14}C]palmitic acid (PerkinElmer Life and Analytical Science, Waltham, MA) for 1 h. The incubation medium was transferred to a vial containing 1 M acetic acid, capped quickly, and allowed to sit for 1 h for the $^{14}CO_2$ gas to be released. $^{14}CO_2$ released was absorbed by hyamine hydroxide, and activity was counted. Fatty acid oxidation was calculated from $^{14}CO_2$ generated. To measure fatty acid uptake, cells were rinsed twice with PBS and lysed after incubation with [1-^{14}C]palmitic acid. Lipids were extracted using a chloroform-methanol mixture (2:1), and ^{14}C counts were determined in the organic phase. Fatty acid uptake was calculated as the total of ^{14}C lipids in the cells and $^{14}CO_2$ generated.

Generation of cells with a hUCP1 reporter system. Immortalized human fat progenitor cells were infected with a lentivirus containing the plasmid, pLV.ExBi.P/Puro-hUCP1promoter-Luc(firefly)-T2A-hrGFP, which expresses luciferase and GFP driven by the human UCP1 promoter. The 4,148-bp human UCP1 promoter was cloned from pLightSwitch_hUCP1-Prom (S723122; Switch Gear Genomics, Carlsbad, CA) and was then subcloned into a lentiviral plasmid to generate a plasmid containing a UCP1 reporter system (Cyagen Biosciences Inc., Santa Clara, CA). 293T cells (ATCC) were transfected with hUCP1promoter-Luc-T2A-GFP, pMD2.G and psPAX2 DNA using PolyJet DNA *in vitro* transfection reagent (SignaGen Laboratories, Rockville, MD). Culture supernatants containing virus were collected every 24 h after infection and filtered through a 0.45 μm filter (Fisher Scientific, Pittsburgh, PA). Immortalized human white and brown fat progenitors at 80% confluence were infected with viral supernatants in the presence of 4 μg/ml Polybrene every day until cells reached 90% confluence. Then cells were treated with 1 μg/ml puromycin in DMEM/H medium containing 10% FBS and antibiotics. Once drug selection was finished, the cells were maintained in culture medium with 0.2 μg/ml puromycin for 2 weeks.

Luciferase reporter assay. *In vitro* luciferase assays were performed using luciferase assay kits (Promega, Madison, WI) according to the manufacturer's instructions. Culture medium from differentiated adipocytes was removed and the cells washed in PBS. An appropriate volume of 1× lysis reagent (passive lysis buffer) was dispensed into each culture well. Cells were scraped from the wells and the lysates transferred into white 96-well plates (Corning Inc., Tewksbury, MA) for detection of the bioluminescence signal using a luminometer plate reader (BioTek Instruments, Inc., Winooski, VT). Reagent injectors were used to dispense 100 μl of luciferase assay buffer with substrate and 100 μl of Stop & Glo reagent. We used a 2-s premeasurement delay followed by a 10-s measurement period for each reporter assay. Luciferase activity data were normalized to protein content.

Time-lapse imaging. Human immortalized cells with hUCP1-promoter-Luc/GFP were plated on a Hi-Q4 culture dish (Nikon, Tokyo, Japan) and cultured in a Nikon BioStation IM-Q (Nikon, Tokyo, Japan), which is a compact cell incubator and monitoring system that allows for live-cell imaging. Cells were maintained in BioStation IM-Q at 37 °C in a 5% CO_2 environment. Adipogenesis was induced as described. Bright-field and fluorescence images were obtained every hour over the course of every 3 d between medium changes for a total of 18 d.

Cell transplantations and *in vivo* luciferase imaging. Human immortalized white and brown fat progenitors with hUCP1-promoter-Luc/GFP were grown in the presence or absence of 3.3 nM BMP7 for 6 d to reach confluence. Cells were washed, trypsinized and resuspended in growth medium with an equal amount of Matrigel Matrix (BD Biosciences, San Diego, CA). Then 1.0×10^7 cells in a 0.3-ml volume were injected into the thoracic-sternum region of 6-week-old male BALB/c athymic nude mice (n = 2 mice for white fat progenitors transplantation group, n = 3 mice for brown fat progenitors transplantation group; Harlan laboratories, Indianapolis, IN) using an 18-gauge needle, according to the methods described previously[23,29]. No statistical method was used to predetermine sample size and experiments were not randomized. For acquisition of the bioluminescence images, the mice were sedated with 2% isoflurane in 100% O_2 in the chamber. D-Luciferin (PerkinElmer Life and Analytical Science, Waltham, MA) was diluted to 3 mg/100 μl in normal saline and 0.6 mg of D-Luciferin was administrated intraperitoneally into mice. An IVIS-Spectrum CT imaging system equipped with a CCD camera (Caliper, PerkinElmer Life and Analytical Science, Hopkinton, MA) was used for *in vivo* bioluminescence imaging. The luminescence intensity in regions of interest from each image was quantified to examine the viability of the implanted cells. Mice were scanned by IVIS each week after transplantation. After 6 weeks of transplantation, mice were sacrificed, and adipose tissue derived from implanted cells was excised and processed for qRT-PCR analysis. There was no blinding during animal experiments. The animal experiment was performed according to procedures approved by the Joslin Diabetes Center Institutional Animal Care and Use Committee (IACUC).

Generation of immortalized clonal cell lines. To derive subclones of immortalized human white and brown progenitors with the hUCP1-promoter-Luc/GFP reporter, limiting dilution of cells into 96-well plates was performed as previously described[27]. Briefly, cells were plated at 50 cells per 96-well plate in DMEM/H containing 10% FBS. After 2 weeks, colonies were evident. Cells at approximately 80% confluence were trypsinized and further propagated in 48-well, then 12-well, and finally 6-well plates. 152 clonal lines that originated from the neck superficial fat depot and 128 clonal lines from deep fat were selected for adipogenic potential after induction. The highly adipogenic clonal lines were selected for further analysis (67 clonal white fat progenitor lines; 90 clonal brown fat progenitor lines).

Microarray analysis. Analysis of gene expression using GeneChip PrimeView (Affymetrix, Santa Clara, CA) was performed on 42 highly adipogenic clonal white and brown cell lines. RNA was isolated from clonal cell lines using Direct-zol RNA miniPrep kit (Zymo Research, Irvine, CA) according to the manufacturer's instructions. The quality of total RNA was evaluated by A_{260}/A_{280} ratio, which was within the value of 1.9 to 2.0 (defined as high quality total RNA). Biotin-labeled cRNA was synthesized, purified and fragmented using GeneChip 3′ IVT Express Kit (Affymetrix, Santa Clara, CA). Integrity and fragmented cRNA was assessed by running aliquots on the Agilent 2100 Bioanalyzer before proceeding further. The high-quality cRNA met the following criteria: the A_{260}/A_{280}fell within the values of 1.9–2.0; the 28S/18S rRNA bands (from the gel) were crisp and the intensity of the 28S band was roughly twice the intensity of the 18S band. As one hWAT-SVF clone had poor cRNA quality, this clone was excluded from analysis. Array hybridization and scanning were performed by the Advanced Genomics and Genetics Core of Joslin Diabetes Center according to established methods. Microarray data were normalized using robust multiarray average (RMA)[50], which placed it on a $\log_2$ scale, and were deposited to the Gene Expression Omnibus (GEO) repository (accession number GSE68544). The log transformation is particularly helpful for making gene expression data approximately normally distributed, so (although we did not explicitly test for normality) the normalized data for each probe set were correlated to $\log_2$(UCP1) using Pearson correlation with a two-sided alternative (with function 'cor.test'), which yielded correlation coefficients and P values. P values were adjusted for multiple testing using FDR[51] with the 'p.adjust' function. The 50 probe sets from unique genes most strongly associated with $\log_2$(UCP1) were plotted in a heatmap along with $\log_2$(UCP1) using the 'heatmap.2' function in the 'gplots' package and color palettes from the 'RColorBrewer' package. The probesets' values were centered to have mean zero and restricted to the interval [−2, 2] to aid visualization, and a color bar representing UCP1 was added at the top, where darker indicates higher UCP1 levels. All microarray analyses were done in the R programming language (http://www.r-project.org).

Engineering target gene–knockout cell clones using the CRISPR-Cas9 system. Cas9 vectors expressing the Cas9 nuclease and guide RNA (gRNA) were obtained from Horizon Discovery Group plc (Cambridge, United Kingdom). Five gRNAs for each target gene were designed using Horizon's proprietary gUIDEbook software and cloned into a Cas9-expressing plasmid on behalf of Horizon by DNA2.0. The plasmid carrying Cas9, gRNA and a GFP selection marker was introduced into the immortalized cell clone by transfection using PolyJet DNA *in vitro* transfection reagent (SignaGen Laboratories, Rockville, MD). On the next day, the cell culture medium was replaced with fresh medium

doi:10.1038/nm.3881

supplemented with 10% FBS, and reseeded when the cells became confluent. To derive subclones with plasmid insertion, we selected and expanded the GFP$^+$ clones, followed by extraction of total RNA for qRT-PCR using standard methods.

Cell sorting. CD29$^+$ progenitors were sorted by FACS, as previously described[23]. Briefly, cells were trypsinized, centrifuged and resuspended in HBSS (Invitrogen, Life Technologies, Carlsbad, CA) with 2% FBS. CD29 antibody (β1-integrin, 1:200, APC conjugate, clone TS2/16; eBioscience, San Diego, CA) incubation was performed for 20 min on ice in HBSS containing 2% FBS. For cell sorting, a Cytomation Moflo (Cytomation, Inc.) instrument was used. FACS data were collected using Summit software (Cytomation, Inc.) and analyzed offline using FlowJo software (TreeStar, Inc., Macintosh version 8.1.1).

Immunofluorescence staining. Cells were grown and differentiated on a chamber covered with a glass slide (Lab-Tek II chamber CC2 glass slide cover; Thermo Scientific, Waltham, MA). Fully differentiated cells were fixed in 4% paraformaldehyde for 10 min and washed three times with PBS. Cells were permeabilized with 0.1% Triton X-100 for 30 min and incubated with UCP1 antibody (1:50, rabbit polyclonal; AnaSpec, Fremont, CA) overnight at 4 °C. After primary antibody incubation, cells were washed and incubated with appropriate secondary antibody (Alexa Fluor 488 (green); Invitrogen, Life Technologies, Carlsbad, CA) at a 1:200 dilution for 10 min in the dark. After secondary antibody incubation, cells were washed with distilled water for DAPI staining (0.1 μg/ml in water for 5 min in the dark), and mounted. Cells were kept in the dark after mounting and analyzed by a fluorescence microscope (Olympus BX60F-3; Olympus Corporation, Tokyo, Japan). Identical conditions and settings were used for picture acquisition and analysis. A threshold was set for each image to eliminate background and to create a binary mode image. For every section and cells, images from three representative areas were analyzed.

Nile red staining. To detect intracellular lipid droplet in live cells, Nile Red staining was performed in differentiated adipocytes. Cells were washed twice in PBS and then incubated in PBS containing 3 μM Nile red (Life Technologies, Carlsbad, CA) for 60 min at 37 °C. Cells were washed with PBS to remove the Nile red working solution and the fluorescence change at $\lambda_{Excitation}/\lambda_{Emission}$ = 552/636 nm was monitored with a fluorescence microscope or fluorescent plate reader (BioTek Instruments, Inc., Winooski, VT).

Statistics. All results were expressed as mean ± s.e.m. All statistical analyses were performed using the programs Excel (Microsoft) and Statview (SAS Institute). Two-tailed Student's *t*-test was used to determine *P*-values. Statistical significance was defined as $P < 0.05$. Gene expression level in human WAT versus BAT was analyzed by using Wilcoxon matched-pairs signed-rank test. No statistical method was used to predetermine sample size. The experiments were not randomized or blinded. Exclusion criteria were as described in the 'Microarray analysis' section above.

50. Irizarry, R.A. *et al.* Exploration, normalization, and summaries of high-density oligonucleotide array probe level data. *Biostatistics* **4**, 249–264 (2003).
51. Benjamin, Y. *et al.* Controlling the false discovery rate: a practical and powerful approach to multiple testing. *J. R. Statist. Soc. B* **57**, 289–300 (1995).